Sensors and Actuators A 158 (2010) 231–239

Contents lists available at ScienceDirect

Sensors and Actuators A: Physical

journal homepage: www.elsevier.com/locate/sna

Experimental analysis and characterization of electrostatic-drive tri-axis micro-gyroscope

Nan-Chyuan Tsai*, Chung-Yang Sue

Department of Mechanical Engineering, National Cheng Kung University, Tainan 70101, Taiwan, ROC

ARTICLE INFO

Article history:
Received 22 August 2009
Received in revised form
22 December 2009
Accepted 4 January 2010
Available online 13 January 2010

Keywords:
Tri-axis micro-gyroscope
Cross-axis perturbation
Sensitivity
Coriolis acceleration

ABSTRACT

A planar micro-machined tri-axis gyroscope in decoupled-mode mechanical structure is presented, verified for superior detection capability and analyzed by experiments in this paper. Initially, the natural frequencies of sense modes are successfully tuned to match the natural frequency of drive mode by polarization voltages onto the associated sensing electrodes so that the inherent bias frequency at each sense mode can be removed. Secondly, the undesired cross-axis coupling effects between drive mode and sense modes are substantially suppressed by the cooperation of mechanical design and an integrated Automatic Gain Control (AGC) loop for drive mode. For highly reliable tuning to ensure resonance, the AGC and PLL (Phase Lock Loop) are integrated with a PID (Proportional, Integral and Differential) feedback controller to eliminate steady-state errors and overshoots. The performance of the micro-gyroscope is analyzed and evaluated by experiments. The achieved scale factors (the reflected voltage to the detected angular rate) of the proposed tri-axis micro-gyroscope are 50.4 μV/°/*s*, 60.3 μV/°/*s*, and 71.2 μV/°/*s* for *X*-, *Y*- and *Z*-axes (principal axis: *Z*-axis) respectively. The resulted resolutions are about 0.72°/s/$\sqrt{\text{Hz}}$, 143°/s/$\sqrt{\text{Hz}}$ and 0.42°/s/$\sqrt{\text{Hz}}$ for *X*-, *Y*- and *Z*-axes respectively. The Cross-axis sensitivities are reduced down to 22%, 9% and 1.84% for *X*-, *Y*- and *Z*-axes respectively. S/N ratios reach 59.3, 13.8, and 140.1 for *X*-, *Y*- and *Z*-axes respectively. The experimental results illustrate that the gyroscope exhibits superior to detect exerted angular rate, in addition to successful suppression upon the cross-axis perturbation between drive mode and sense mode. Principle-axis sensitivity, resolution and floor noise are all numerically evaluated. Further more, cross-axis sensitivity, Signal-to-Noise Ratio (SNR) and measurement error are investigated. Finally, a few comparisons with the other typical types of gyroscopes are reported.

1. Introduction

Micro-machined gyroscopes, used to measure exerted angular velocity, attracted a lot of attention during the past decade owing to fairly tiny size and low cost. For industries, micro-gyroscopes can be applied for car rollover detection, motion control of robotics, attitude control of micro-satellites, and prevention of wheelchair turn-over. For consumer electronics, micro-gyroscope can be utilized for video-camera stabilization, cell-phone posture detection and video game consoles (such as PS3, Verizon and Xbox 360) [1]. By angular rate detection capability, micro-gyroscope can be classified into single-axis, dual-axis and tri-axis types. "*Single-axis*" means that solely one axis angular rate (*X*-, *Y*-, or *Z*-axis) can be measured by the gyroscope. Similarly, "*dual-axis*" and "*tri-axis*" micro-gyroscope implies that two and three mutually perpendicular angular velocities can be simultaneously measured respectively. Basically, single-axis and dual-axis micro-gyroscopes are already well developed and successfully employed in many industries because the associated MEMS techniques (e.g., surface micro-machining) have been sufficiently mature [2–5]. Therefore, superior-performance tri-axis micro-gyroscopes is expected to be developed in the near future. However, though a few tri-axis micro-gyroscopes were ever reported recently but some key issues remain unsolved. For example, John and Vinay [6] proposed a tri-axis micro-gyroscope in which only a single proof mass is used as the detection element. However, by using a single proof mass to detect three mutually perpendicular angular velocities, the coupling effects upon the measured data have to be effectively reduced at first. Chou et al. [7,8] reported a hemispherical shell micro-gyroscope that was capable to measure three-axis angular rates simultaneously. However, more complicated 3D micro-machining processes are definitely necessary to construct the hemispherical shell and the associated electrical connections. Moreover, the fabrication process is incompatible with the conventional CMOS-MEMS process. For more details of typical tri-axis micro-gyroscopes will be discussed in Section 6.3.

In our previous works, a planar tri-axis micro-gyroscope by using conventional SOI (Silicon on Insulator) fabrication process

* Corresponding author. Tel.: +886 6 2757575x62137; fax: +886 6 2369567.
E-mail address: nortren@mail.ncku.edu.tw (N.-C. Tsai).

0924-4247/$ – see front matter © 2010 Elsevier B.V. All rights reserved.
doi:10.1016/j.sna.2010.01.005

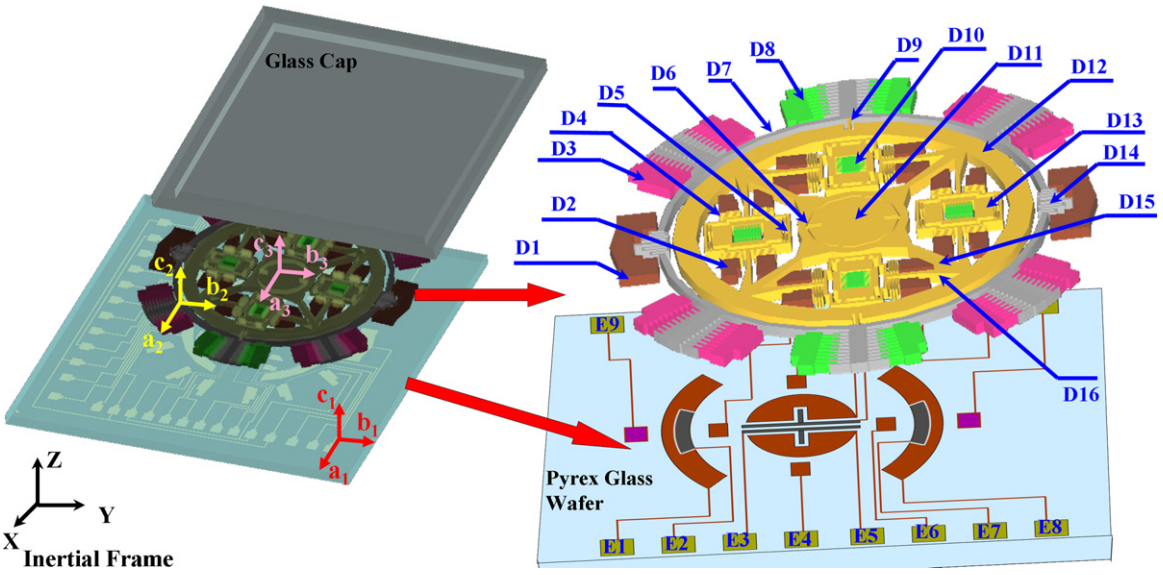

Fig. 1. Studied tri-axis micro-gyroscope and coordinate systems. $\langle X, Y, Z\rangle$: inertia frame, $\langle a_1, b_1, c_1\rangle$: chip frame, $\langle a_2, b_2, c_2\rangle$: oscillatory ring twister frame, $\langle a_3, b_3, c_3\rangle$: Outer-ring frame.

was proposed [9–12]. In this paper, an innovative micro-structure design of tri-axis micro-gyroscope is proposed to improve the drive efficacy. An AGC (Automatic Gain Control) loop is included so that the measurement capability on angular rate by the actual micro-chip can be upgraded. Most importantly, the performance of the novel gyroscope is evaluated by experiments, instead of computer simulations or theoretical analysis.

2. Operation principle and fabrication of tri-axis micro-gyroscope

2.1. Design and operation

The studied tri-axis micro-gyroscope is schematically shown in Fig. 1. There are eight sets of key components, as listed in Table 1, for the electrostatic-drive tri-axis micro-gyroscope. In order to describe the operation of the studied gyroscope, four coordinate systems, $\langle X, Y, Z\rangle$, $\langle a_1, b_1, c_1\rangle$, $\langle a_2, b_2, c_2\rangle$ and $\langle a_3, b_3, c_3\rangle$ are introduced (see Fig. 1). $\langle X, Y, Z\rangle$ is the inertial frame (i.e., the absolute coordinate). Coordinate $\langle a_1, b_1, c_1\rangle$ is attached to the substrate and hereafter named as "*chip frame*". Since the gyroscope is always driven to be oscillatory, coordinate $\langle a_2, b_2, c_2\rangle$, named as "*ORT frame*" in this paper, is defined as the attached frame at the Oscillatory Ring Twister (ORT). To describe the relative motions between the components, $\langle a_3, b_3, c_3\rangle$ is attached to Outer-ring and named as "*Outer-ring frame*" so that the induced displacements of the detection modules can be well described to ORT frame. The corresponding angular displacements of the detection components, based on the aforesaid coordinates, are $\langle\theta_x, \theta_y, \theta_z\rangle$, $\langle\alpha_1, \beta_1, \gamma_1\rangle$, $\langle\alpha_2, \beta_2, \gamma_2\rangle$ and $\langle\alpha_3, \beta_3, \gamma_3\rangle$ respectively. For drive mode operation, ORT (D7) is driven by the rotational comb-drive electrodes (D3) to rotate, within a limited interval, counter clockwise and clockwise alternatively about c_1-axis. That is, ORT is oscillatory about c_1-axis. On the other hand, Outer-ring, Inner-disk and Distributed Translational Proof Masses (DTPMs) are the three seismic inertial masses marked as D11, D12 and D13 in Fig. 1 respectively. In fact, the seismic inertial masses are the angular rate detection components whose responding motions are all induced by Coriolis effect. It is noted that the Outer-ring is connected to Oscillatory Ring Twister by springs (marked as "D9" in Fig. 1), while Inner-disk and DTPM are connected to Outer-ring by ribs (marked as "D16" and "D15" in Fig. 1 respectively). Therefore, Outer-ring, Inner-disk and DTPM are concurrently subject to vibratory drive about c_1-axis. Totally five spring sets are designed (marked as D4, D5, D6, D9 and D14 in Fig. 1). The first set is named as *S1* (marked as D14 in Fig. 1) which is utilized to suspend ORT and, by mechanical design, only allow the rotary motions of Oscillatory Ring Twister about c_1-axis. Outer-ring is suspended by a set of torsion springs, named as Spring *S2* (marked as D9 in Fig. 1). Similarly, Inner-disk is suspended by the torsion spring set, *S3* (marked as D6 in Fig. 1). Spring *S4* and Spring *S5* (marked as D4 and D5 in Fig. 1) are respectively used to resist the tangential and radial acceleration of DTPMs. The sensing capacitor sets consist of two pairs of parallel plate differential capacitors (marked as E1 and E5 in Fig. 1) and two pairs of comb-electrodes differential capacitors (marked as D8 and D10 in Fig. 1). The induced pitches of Outer-ring and Inner-disk, w.r.t. equilibrium position, are detected by the parallel plate differential capacitors E1 and E5 respectively. A pair of comb-electrode differential capacitors, D10, is used to measure the radial motion of DTPM induced by Coriolis acceleration. Another pair of comb-electrode capacitor pairs, D8, is used to monitor the rotary motion of Oscillatory Ring Twister so that the expected spinning speed can be achieved by the drive feedback loop. On the other hand, the tuning electrodes, E2 and E3, are used for frequency tuning for Outer-ring and Inner-disk respectively to ensure that the corresponding resonance can really occur.

Theoretically, all of the seismic inertial mass modules are driven into resonance about c_1-axis at first. Once the exerted angular rate was about *X*-axis (i.e., $\vec{\omega} = \omega_x\hat{i}$), Inner-disk would respond to oscillate about b_3-axis (i.e., β_3-direction) by Coriolis effect. It is noted that the so-called "exerted angular rate" in this paper is referred to the angular rate which is to be detected by the gyroscope. Similarly, Outer-ring would respond to oscillate about a_2-axis, due to Coriolis effect, if the exerted angular rate was about *Y*-axis (i.e., $\vec{\omega} = \omega_y\hat{j}$). The induced pitch of Inner-disk or Outer-ring is then measured by the associated differential capacitor pair, E5 or E1, respectively. Since the Outer-ring and Inner-disk are sandwiched individually by a pair of differential capacitors, the induced pitch of Outer-ring or Inner-disk, with respect to the equilibrium position, results in change of voltage output across the corresponding capacitors. This voltage change can be thus converted as the measure of the exerted angular excitation. On the other hand, DTPM would be forced to oscillate in radial direction if the exerted angular rate was about *Z*-axis (i.e., $\vec{\omega} = \omega_z\hat{k}$). The resulted radial motion of DTPM is measured